Nanoscale

ROYAL SOCIETY OF CHEMISTRY

MINIREVIEW

View Article Online
View Journal | View Issue

Cite this: *Nanoscale*, 2023, **15**, 450

Transformation mechanism of high-valence metal sites for the optimization of Co- and Ni-based OER catalysts in an alkaline environment: recent progress and perspectives

Chen Qiao,[a,b] Yingying Hao,[b] Chuanbao Cao *[b] and JiaTao Zhang *[a,b]

Received 18th October 2022,
Accepted 4th December 2022

DOI: 10.1039/d2nr05783b

rsc.li/nanoscale

As an important semi-reaction process in electrocatalysis, oxygen evolution reaction (OER) is closely associated with electrochemical hydrogen production, CO_2 electroreduction, electrochemical ammonia synthesis and other reactions, which provide electrons and protons for the related applications. Considering their fundamental mechanism, metastable high-valence metal sites have been identified as real, efficient OER catalytic sites from the recent observation by *in situ* characterization technology. Herein, we review the transformation mechanism of high-valence metal sites in the OER process, particularly transition metal materials (Co- and Ni-based). In particular, research progress in the transformation process and role of high-valence metal sites to optimize OER performance is summarized. The key challenges and prospects of the design of high-efficiency OER catalysts based on the above-mentioned mechanism and some new *in situ* characterizations are also discussed.

1. Introduction

With the further development of solar power generation, wind power generation, hydroelectric power generation and other technologies, the cost of green electricity is further reduced, providing new opportunities for power generation using an electrochemical energy conversion technology.[1–6] The high efficiency of electrocatalysis for energy conversion and its utilization was regarded as one of the important ways to solve the energy crisis.[7–12] The development of an electrochemical energy conversion technology not only contributes toward environmental protection but also raises expectations to become economically competitive.[13–18]

Electrocatalysis not only could achieve efficient energy conversion, but also could transform some low-value resources

[a]*MOE Key Laboratory of Cluster Science, School of Chemistry and Chemical Engineering, Beijing Institute of Technology, Beijing 100081, China. E-mail: cbcao@bit.edu.cn, zhangjt@bit.edu.cn*
[b]*Beijing Key Laboratory of Structurally Controllable Advanced Functional Materials and Green Applications, School of Materials Science and Engineering, Beijing Institute of Technology, Beijing 100081, China*

Chen Qiao

Chen Qiao obtained his doctorate from Beijing Institute of Technology (BIT), China. He is currently a postdoc of the School of Chemistry and Chemical Engineering, BIT. His main research interests include the preparation of two-dimensional nanomaterials and design of high-efficiency electrocatalysts.

Yingying Hao

Yingying Hao received her bachelor's degree from Henan University (HENU), China. She is currently pursuing her master's degree at Beijing Institute of Technology. Her main research interests include the synthesis of electrocatalysts and their applications in electrocatalytic energy.

into useful chemical products.[19–24] As important half-reactions, OERs are often overlooked by laymen because they do not yield useful chemical products such as H_2, NH_3, and CO. In fact, OERs provided protons and electrons in the overall catalytic system, which was related to the overall efficiency of the electrochemical reaction.[25–31] The OER involved a four-electron transfer process leading to its kinetic depression. This might lower the efficiency of the overall reaction, but OER catalyst optimization for the overall reaction has a huge room for improvement.[32–37]

In this review, based on the conventional mechanism of OERs, we further introduce the specific catalytic mechanism of Co- and Ni-based catalysts in detail. The relationship between the transformation of high-valence metal sites in the OER process and efficient OER catalysis was explored based on *in situ* characterization technology and theoretical calculation models. Recent progress in the transformation mechanism of high-valence metal sites for OERs is emphasized. Finally, the prospects and challenges of research on the transformation mechanism of high-valence metal sites for the optimization of OER catalysts are presented.

2. OER mechanism

OER mechanism is the basis of designing excellent catalysts. At present, the mechanism of OERs in an alkaline environment mainly includes adsorption evolution mechanism (AEM) and lattice oxygen evolution mechanism (LOM). As shown in Fig. 1a, the AEM mechanism consists of four successive electron transfer steps, and the reaction involves three reaction intermediates (*OH, *O, and *OOH).[38] Specifically, the metal active site first completes the adsorption of OH^- to form M–*OH accompanied by the transfer of one electron (step1). Then, there occurs simultaneous transfer of electrons and protons on the M site from M–*OH to M–*O (step 2), M–*O further reacts with OH^- to get M–*OOH (step 3), and finally, releases O_2 and H_2O by interacting with OH^- and the clean M active site was obtained (step 4). Based on the AEM, the activity of the catalyst was closely related to the adsorption energy between the metal active site and the intermediate. Therefore, there is a theoretical possibility that the optimal catalyst would be achieved by regulating the adsorption energy consistency between the four steps of the reaction.[3,39,40] Density functional theory (DFT) calculations were used to assess the intermediate energy between each reaction step. To reduce the difficulty of obtaining the transition state energy, the Brønsted–Polanyi–Evans (BEP) relation was proposed.[41–43] The BEP relation assumes that the activation barrier is proportional to the internal energy barrier. This means that the kinetics in the experiment could be predicted by thermodynamics.[44] At present, the DFT calculation is widely used in the research of OERs.[3]

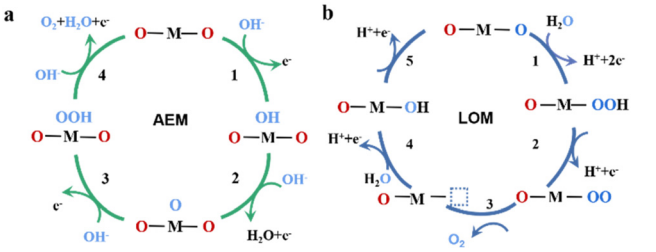

Fig. 1 (a) Conventional AEM mechanism. (b) LOM mechanism.

However, in the reaction path of LOM, O–O coupling occurs directly on lattice oxygen, which is directly involved in oxygen precipitation, rather than on the M–metal site in the AEM. This implies that this pathway is not limited to the adsorption energy proportional relationship in the AEM pathway (Fig. 1b). Although LOM had the potential to increase the activity of

Chuanbao Cao

Chuanbao Cao is currently professor at the School of Materials Science and Engineering, Director of Research Center of Materials Science of Beijing Institute of Technology, China. His research is focused on the electrochemical energy storage and conversion including electrode materials of lithium ion batteries, supercapacitors, catalysts and photo-electrochemical materials. Until now, he has published more than 380 peer-review research papers, holds or has filed 50 patents.

JiaTao Zhang

Jiatao Zhang was born in 1975. He earned his PhD in 2006 from Tsinghua University, China. Currently, he is Xu Teli Professor in Beijing Institute of Technology. He was awarded Excellent Young Scientist foundation of NSFC in 2013. He also serves as the Dean of the School of Chemistry and Chemical Engineering and the Director of Beijing Key Laboratory of Construction-Tailorable Advanced Functional Materials and Green Applications. His current research interest is focused on inorganic chemistry of semiconductor-based hybrid nanostructures possessing novel optical, electronic properties for applications in energy conversion and storage, catalysis, optoelectronics and biology.

OERs, the involvement of lattice oxygen would seriously affect the stability of the catalyst.[45]

Based on the OER mechanism, the adsorption capacity of the reaction intermediates on the active site could affect the ability of the catalyst to oxidize water. In recent years, transition metal (TM) materials have been considered as promising catalysts due to their unique d-orbital properties.[46–48] In addition, because of their low cost and environmental friendliness, they gradually replaced the traditional noble metal.[49,50] In the last decade, due to diversity in the electronic structure of TM materials, such as charge amount, charge distribution and spin state, more opportunities have been provided for catalyst design. In particular, TM hydroxide/hydroxyl oxide has become a hot topic in OER research.[51–54]

3. Operando identifying Co- and Ni-based OER catalyst active phase

The design of efficient catalysts is inseparable from the related mechanistic studies. Understanding the reaction mechanism of specific catalysts is considered necessary to design more efficient catalysts. In recent years, an increasing number of *in situ* characterization technologies have been used in the study of related mechanisms.[55] *Via* the *in situ* characterization technology, the transformation of the catalytic site during the catalytic process can be monitored to get closer to the truth of the catalytic reaction.[38] Benefiting from the development of *in situ* characterization technology, the high-valence state transformation process on metal sites during the OER process has been revealed, and further mechanistic studies have been carried out.[56,57] Raman spectrum and X-ray absorption spectroscopy (XAS) techniques have been widely used in the field of *in situ* characterization.[58] Raman spectroscopy is a vibration spectroscopy technique with high sensitivity in the low frequency range and high molecular specificity. Particularly for catalysts, the observation of the vibrational location of M–OH, M–OH_2, and M=O was of great significance for the research of reconstruction and adsorption of intermediates.[59,60] In addition, Raman technology with non-interference of water is suitable for *in situ* monitoring of intermediates in electrochemical systems in water-based media. XAS is inner-shell spectroscopy that provided detailed information about the local atomic structure, coordination environment, chemical bonds, and oxidation states of materials.[60,61] These information provided valuable evidence for the study of catalyst mechanism.

Bin Liu *et al.*[62] determined the roles of different Co sites in spinel Co_3O_4 in the OER process by *operando* X-ray absorption spectroscopy and electrochemical characterization techniques. One Co(II) in the tetrahedral site (Co(II) Td) has been confirmed to be transformed into CoOOH as the active site of water oxidation, while Co(III) in the octahedral site (Co(III) Oh) provided –OH adsorption, which induced double-layer capacitance favoring the overall catalytic process. Shuo Zhang *et al.*[63] used the *operando* X-ray absorption spectroscopy to reveal that a potential-dependent deprotonation reaction occurs during the OER, and $Co^{3+}/^{4+}OOH_{1-x}$ transformed at high potentials was identified as the active phase of OERs (Fig. 2a). The relationship between the OER activity and deprotonation energy was suggested to be a descriptor, which provides a basis for further mechanism interpretation and design of related catalysts. Xile Hu *et al.*[64] revealed the mechanism of CoOOH OER by *in situ* X-ray absorption and Raman spectroscopy. *Via in situ* X-ray absorption (XAS) technology (Fig. 2b), when the applied potential reached 1.45 V, traces of Co(IV) converted by Co(III) appeared on the surface of the material, and when the applied potential reached 1.55 V, the oxidation state of Co on the surface showed a slight increase, implying that the proportion of Co(IV) sites on the surface increased. Further isotope labeling results confirmed that Co (IV) is the confirmed site of oxygen precipitation. Thomas J. Schmidt *et al.*[65] demonstrated the relevant mechanism of $Ba_{0.5}Sr_{0.5}Co_{0.8}Fe_{0.2}O_{3-\delta}$ as the OER catalyst. The formation of the (Co/Fe)O(OH) self-assembled active layer was due to the lattice oxygen evolution reaction (LOER)/OER mechanism. *In situ* XAS results revealed that the valence of Co increased with the increase in applied potential.

The efficient OER performance of Ni-based materials is closely related to the collaboration of Fe. The excellent performance of NiFe-LDH materials has attracted extensive attention. In particular, the research in the reaction mechanism was considered to be an effective means of further optimization of relevant OER catalysts.[66,67] Among many influencing factors, the identification of the active site was considered to be an important breakthrough to reveal the OER mechanism of the bimetallic catalyst NiFe-LDH. At the beginning of the research, due to the limitation of the measurement technology, the high-valence state transformation of Ni and Fe in the OER process was not realized, which also meant that it was difficult to approach the truth of the efficient catalysis of NiFe-LDH. Speculation was used for relevant mechanism explanations until the introduction of *in situ* characterization techniques. Alexis T. Bell *et al.*[68] revealed that the catalyst NiFe-LDH exhibited different valences under different applied overpotentials *via in situ* XAS (Fig. 2c). When the applied overpotential was lower than the onset overpotential, Ni would change from Ni(II) to Ni (III), and with the increase in applied potential, Fe(III) would change to Fe(IV). Further combined with the proposed calculation model, compared with Ni, Fe sites showed better adsorption energy of OER intermediates. Fe was inferred to be the main catalytic site in NiFe-LDH. Shannon S. Stahl *et al.*[69] by *in situ* Mössbauer spectroscopy showed the transformation of Fe (III) to Fe(IV) at high potentials during the OER process for NiFe-LDH. The research confirmed the indispensable contribution of Fe(IV) in the OER, revealing that Fe(IV) is not related to the OER activity (Fig. 2d). Dongniu Wang *et al.*[70] reported the increase in the oxidation state of Ni from Ni(III) to Ni (3.6) and the appearance of a highly covalent Fe(IV)–O bond under the operating potential by *in situ* X-ray absorption near-edge structure (XANES) spectroscopy. Peter Strasser *et al.*[71] reported that when the applied potential reached 1.63 V, the results of *in situ* XAS tests revealed a change in Ni atoms from Ni(II) to Ni(III) (+3.7),

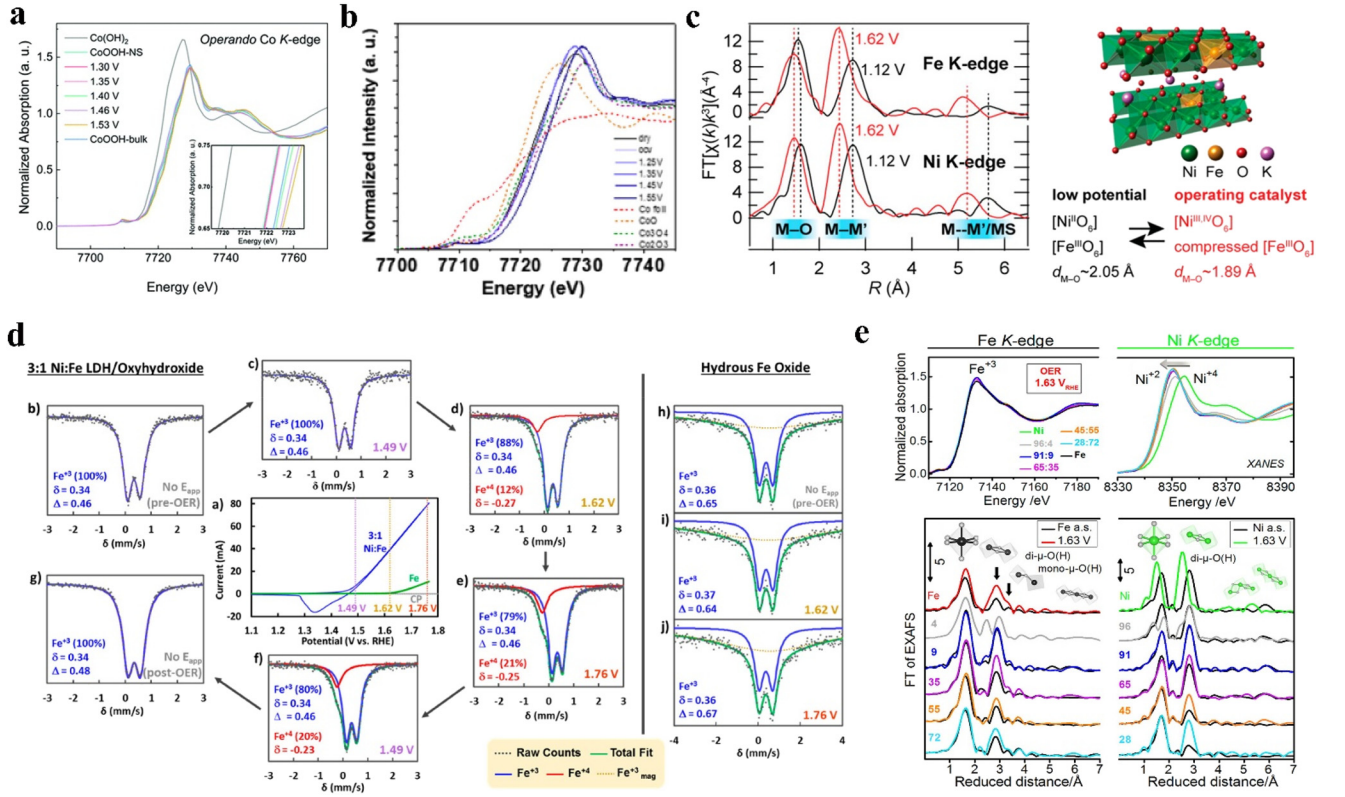

Fig. 2 (a) Operando Co K-edge spectra of CoOOH-NS during potential holding from open circuit to 1.53 V *vs.* RHE in 1 M KOH. Reproduced with permission from ref. 63: Copyright 2019 Royal Society of Chemistry. (b) XANES spectra of CoOOH at various potentials, as well as reference samples Co foil (red), CoO (brown), Co_3O_4 (green), and Co_2O_3 (purple). Reproduced with permission from ref. 64: Copyright 2020, American Chemical Society. (c) Complementary *operando* EXAFS measurement confirming the potential-induced bond contraction at both Fe and Ni sites and structure model of Fe-doped γ-NiOOH. Reproduced with permission from ref. 68: Copyright 2015, American Chemical Society. (d) CVs of NiFe-layered oxyhydroxide (blue) and hydrous Fe oxide (green) electrocatalysts used for the *operando* experiments with the Mössbauer spectra collected at open circuit (gray), at 1.49 V (purple), 1.62 V (yellow), and 1.76 V (red). CV data were recorded in a Mössbauer electrochemical cell at a scan rate of 25 mV s^{-1} prior to Mössbauer measurements. Reproduced with permission from ref. 69: Copyright 2015, American Chemical Society. (e) X-ray absorption spectra of the Ni–Fe catalysts with different catalyst compositions ($Ni_{100-x}Fe_x$) freeze-quenched under the application of catalytic potential after conditioning at 1.63 V for 30 min in 0.1 M KOH. Reproduced with permission from ref. 71: Copyright 2016, American Chemical Society.

suggesting that the catalyst achieved a γ-NiOOH phase transformation at the current potential, which is consistent with previous reports (Fig. 2e). However, different from previous reports, it was found that the existence of Fe(III) was not affected by the potential, and the existence of Fe(III) was conducive to the stability of the overall crystal structure.

Due to the differences in test conditions, it was still difficult to get acceptable results to explain the changes and roles of Ni and Fe sites in the reaction process even with *in situ* characterization technology. However, the Ni–Fe bimetallic system was more complex than the Co-based material, which greatly increased the difficulty in related research. Researchers tried to find a breakthrough *via* DFT calculations at a theoretical level. William A. Goddard III *et al.*[72,73] reported that the OER mechanism of O–O coupling and O_2 release in NiOOH and NiFe-OOH was investigated based on a state-of-the-art theoretical method. The formation of an active O radical species and the subsequent O–O coupling were considered to be key steps in determining the OER catalytic performance of NiOOH and NiFe-OOH. The high-spin Fe(IV) site transferred O radicals more easily than the Ni site, while reducing the O–O coupling barrier on the Ni(IV) site (Fig. 3). Therefore, the synergistic effect of Ni and Fe was confirmed, which was the key

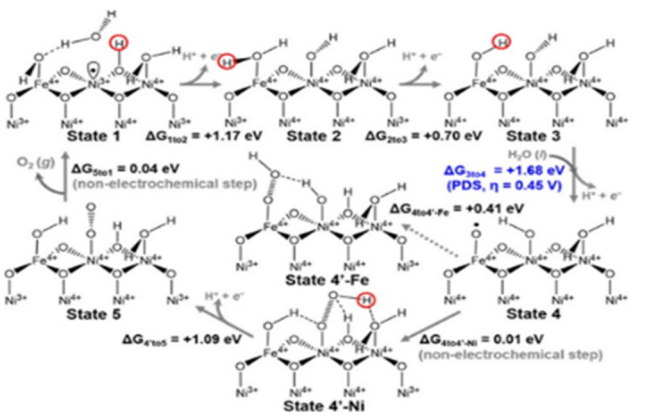

Fig. 3 Mechanism of the OER on the $Ni_{1-x}Fe_xOOH$ catalyst leading to η = 0.45 V. Reproduced with permission from ref. 73: Copyright 2018, American Chemical Society.

factor for the excellent OER performance of NiFe-based materials. It was worth noting that high-value Ni and Fe were directly used in the calculation. Previous studies have revealed that high-value Ni and Fe were difficult to achieve without applied potential. This means that the search for an efficient oxidation process was inseparable from the high-value transformation of metal active sites. Therefore, it is considered to be an excellent idea for the catalyst design to find an effective way to construct the high active site at low overpotentials.

4. High-valence metal site construction

The increase in valence was accompanied by a change in the material structure, which is clearly captured by *in situ* XAS results. The oxidation of M(II) to M(IV) comprises the following reactions:[74,75]

$$M(II) + 2(OH)^- \rightarrow M\text{–}OOH + H^+ + e^- \quad (1)$$

$$M\text{–}OOH \rightarrow MO_2 + H^+ + e^- \quad (2)$$

This structural transformation process has been widely reported in sulfides, phosphates, hydroxides, *etc.*[55,64,75] Despite Co(IV)[2] and Ni(IV)[76] been confirmed that the reaction sites of high-valence in the process of water oxidation determined the final catalytic performance. The direct construction of high-valence Co/Ni sites is still impossible. Fortunately, there are a few reports to achieve the transformation of Co(IV)/Ni(IV) at low overpotentials by means of additional active sites,[77] metal doping,[76,78] and anion modification.[79]

Benefiting from the controllable preparation of relevant materials, studies on metal doping have been reported. Yang Chai *et al.*[76] showed that highly oxidized Ni(IV) appeared on multicomponent FeCoCrNi alloy films by a multistep oxidation process (Ni(II) → Ni(III) → Ni(IV)). The introduction of Fe components was considered to be the main factor in inducing the multistep oxidation process, which avoided the limitation of the high energy barrier required for the original conversion to Ni(IV). Zhiyong Tang[80] revealed the influence caused by different metal ratio pairs on the valence transformation of metal sites. The catalyst was synthesized by adjusting the ratio of Ni and Co in NiCo-MOF-74. The *operando* XAS results revealed that the transformation of high-valence Ni at a low applied potential could be achieved by adjusting the ratio of metal. Zhichuan J. Xu *et al.*[81] showed that the role of Fe in $CoFe_{0.25}Al_{1.75}O_4$ would induce highly active hydroxyl oxide

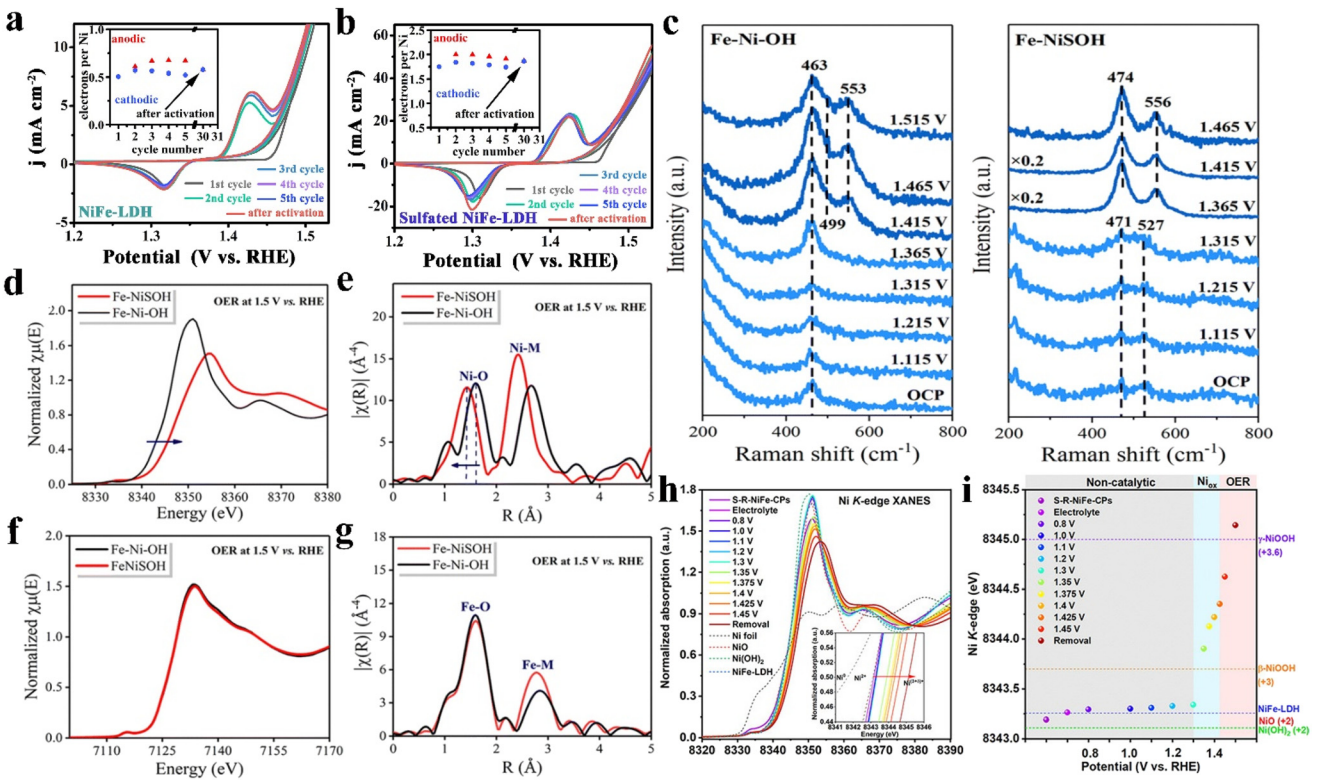

Fig. 4 (a) CV curves of NiFe-LDH nanosheets; inset: electrons transferred per Ni atom. (b) CV curves of sulfated NiFe-LDH nanosheets; inset: electrons transferred per Ni atom. Reproduced with permission from ref. 79: Copyright 2021, Elsevier Inc. (c) Schematic illustration of the *in situ* Raman experiment set-up. *In situ* Raman spectra and normalized (d) Ni and (f) Fe K-edge XANES spectra at 1.5 V *vs.* RHE in a 1 M KOH aqueous solution, and (e and g) corresponding k^3-weighted FT-EXAFS spectra without phase-shift correction for freshly prepared Fe-NiSOH and Fe–Ni–OH electrodes. Reproduced with permission from ref. 82: Copyright 2022 Royal Society of Chemistry. (h) Operando Ni K-edge XANES spectra of *SR*-NiFe-CPs at different anodic potentials in 0.1 M KOH for the OER (i) Ni K-edge positions *vs.* applied potentials. Reproduced with permission from ref. 83: Copyright 2022, American Chemical Society.

reconstruction. Thus, it was inferred that Fe could activate Co preoxidation at low potentials, promoting surface reconstruction and subsequent activation of active sites. The key role of Fe was to promote the deprotonation process and generate reactive oxygen species at a lower potential on $CoFe_{0.25}Al_{1.75}O_4$, thereby improving the catalytic performance of the OER.

Additional active sites were considered as an opportunity for the construction of high-valence sites. Xi Wen Du[77] *et al.* reported an optimization strategy for the introduction of additional active sites. Different from the single adsorption of intermediates by ordinary catalysts (NiO or NiFe-LDH), in NiO/NiFe LDH, one or two additional chemical bonds always assisted the nickel cation adsorption of intermediates, forming a unique 3D adsorption, which resulted in the presence of a Ni(IV) site at the NiO/NiFe LDH junction.

Anion modification was also proved to be an effective method for the construction of high-valence metal sites at the low potentials. Our team reported that NiFe-LDH nanosheets modified with sulfate could achieve an efficient O–O coupling process at low potentials.[79] It was found that sulfate modification enhanced the oxidation states of Ni and Fe sites during the reconstruction process of the material, and further confirmed that the oxidation peak at low overpotentials was not only attributable to the oxidation process of Ni, but also included the O–O coupling process on the Ni site by fitting the transfer electron number of electrochemical tests (Fig. 4a and b). The efficient O–O coupling at low overpotentials caused by the construction of high-valence metal sites was considered to be the main factor for the high efficiency of catalysts. Similar results were also shown by Ying Yu *et al.* The research mainly focuses on Fe-NiSOH. As shown in Fig. 4c, *in situ* Raman results indicated that the trigger potential of $Ni(OH)_2$ to NiOOH transformation on Fe-NiSOH (1.365 V) was lower than that of the Fe–Ni–OH catalyst (1.415 V). Further *in situ* XAS results revealed that for the Ni K-edge XANES spectrum, the absorption edge of the Ni XANES spectrum in the Fe-NiSOH catalyst exhibited a positive shift of ~2.7 eV compared with that in the Fe–Ni–OH catalyst, which was attributed to the change from Ni(II/III) to Ni(III/IV) (Fig. 4d–g).[82] Greta R. Patzke *et al.*[83] reported a related study on sulfide reduction of the NiFe coordination polymer (*S-R*-NiFe-CP). The Ni K-edge XANES spectra of *S-R*-NiFe CPs at applied potentials between 0.8 and 1.45 V *vs.* RHE were recorded. Three different reaction processes were found in the range of applied potentials. At the non-catalytic potential (0.8–1.3 V *vs.* RHE), the valence of Ni ions mainly corresponds to Ni(II). At the Ni oxidation potential (1.3 V to 1.425 V *vs.* RHE), energy shift of the absorption edge is caused by the oxidation of Ni ions. With the applied potential increased to above 1.425 V *vs.* RHE, high-valence Ni ions are gradually formed on the catalyst (Fig. 4h and i). Combined with the computational results, the researchers believe that the targeted S-atom modification plays a key role in the optimization of the local electronic structure and adsorption energy of OER intermediates on *S-R*-NiFe-CP.

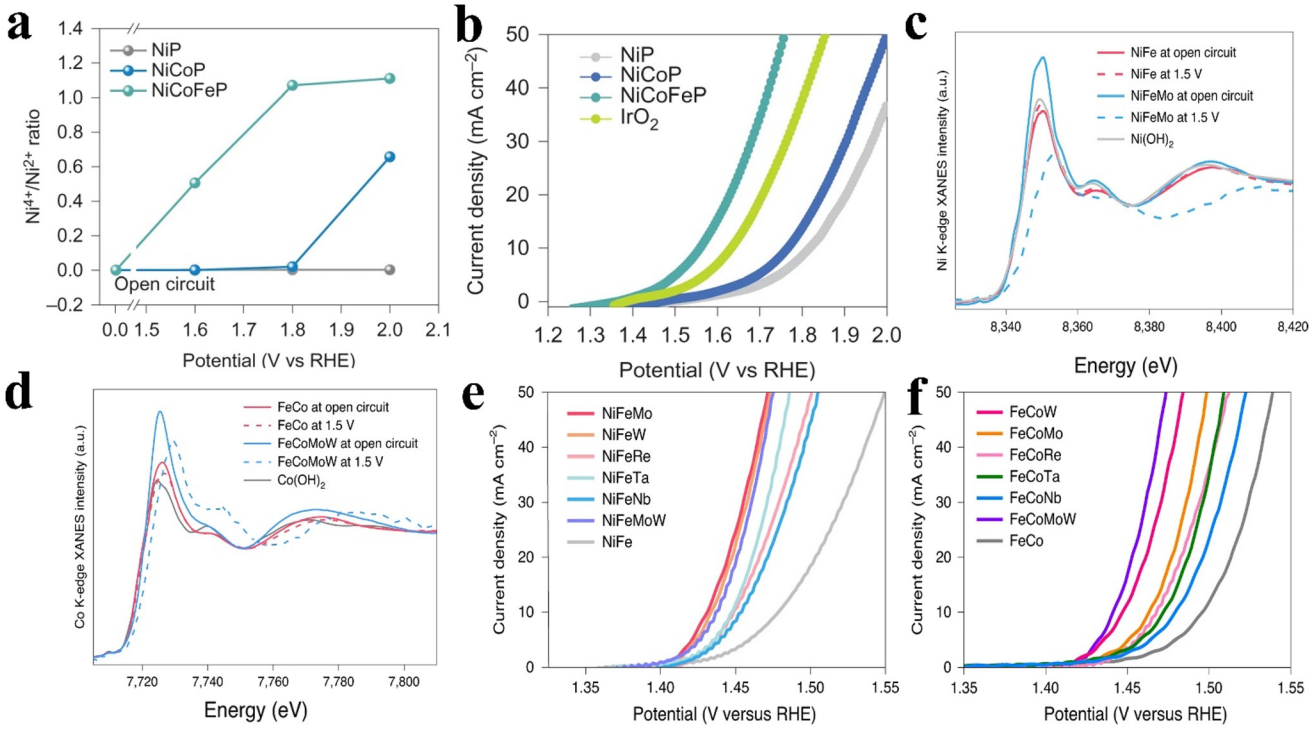

Fig. 5 (a) Ni^{4+}/Ni^{2+} ratio *versus* potential for NiCoFeP and controls. (b) OER polarization curve of catalysts loaded on a Au foam at a scan rate of 1 mV s^{-1}. Reproduced with permission from ref. 58: Copyright 2018, Springer Nature. (c) *In situ* Co K-edge XANES spectra of FeCo and FeCoMoW. (d), *In situ* Ni K-edge XANES spectra of NiFe and NiFeMo. OER polarization curves of NiFeX catalysts (e) and FeCoX catalysts (f). Reproduced with permission from ref. 78: Copyright 2020, Springer Nature.

The relevant research also wanted to find out the relevant descriptors by means of theoretical calculation to further provide favorable support for the mechanism interpretation and catalyst design. The relationship between the OER activity and deprotonation energy was suggested to be a descriptor, which provided a basis for further mechanism interpretation and OER catalyst design. Edward H. Sargent *et al.*[75] synthesized NiCoFeP hydroxyl oxides by simulating that Co, Fe and P doping could reduce the Gibbs formation energy of Ni (IV). Specifically, the reaction free energy of Ni(II) → Ni(III) transform was reduced by the substitutional doping of phosphorus, while the Ni(III) → Ni(IV) reaction free energy was decreased by the substitution of Co and Fe, and Co and Fe doping were considered to be beneficial for the stability of the Ni(IV) phase. To investigate the electronic structure tuning of the catalyst by TM doping, PDOS results indicated that the valence band maximum (VBM) of NiCoFeP was 0.17 eV below the Fermi level of NiO_2, which was lower than that of $Ni(OH)_2$ (0.20 eV), indicating that Ni(IV) had more exposed hole states for catalysis (Fig. 5a and b). In addition, this group continues to report work based on the construction of high-valence sites. A strategy to reprogram the oxidation cycle of Fe, Co, and Ni by combining high-valence transformation metal modulators X (X = W, Mo, Nb, Ta, Re, and MoW) found that in high-valence metal modulation systems, the energy barrier of oxidation transformation in the ternary metal system (such as NiFeMo and FeCoMoW) was lower than that in the binary system (such as NiFe and FeCo) (Fig. 5c–f).[78] Further combined with the corresponding OER performance, these results were consistent with previous reports that 3d metal oxides with lower oxidation barriers have higher OER activity. Wei Luo *et al.*[55] revealed that a new descriptor (intermolecular energy gap, Δ_{inter}) for the formation of Co(IV) species was proposed (Fig. 6a–c). The various cobalt sulfides (CoSα) with amorphous CoOOH layers on the surface were provided as the research object. Δ_{inter} is defined as the energy difference between the valence band maximum (VBM) of CoOOH and the conduction band minimum (CBM) of CoSα. The decrease in Δ_{inter} is beneficial for the formation of Co(IV). For the common transformation from CoOOH to metastable CoO_2, the enhanced d–d coulombic interaction resulted in thermodynamically unfavorable conditions. Co–X with a low CBM level was conducive to the transfer of electrons from CoOOH to CoS, accelerating the formation of Co(IV) (Fig. 6a–c). These results are consistent with the final OER performance, and $CoOOH/Co_9S_8$ showed the best OER performance (Fig. 6d).

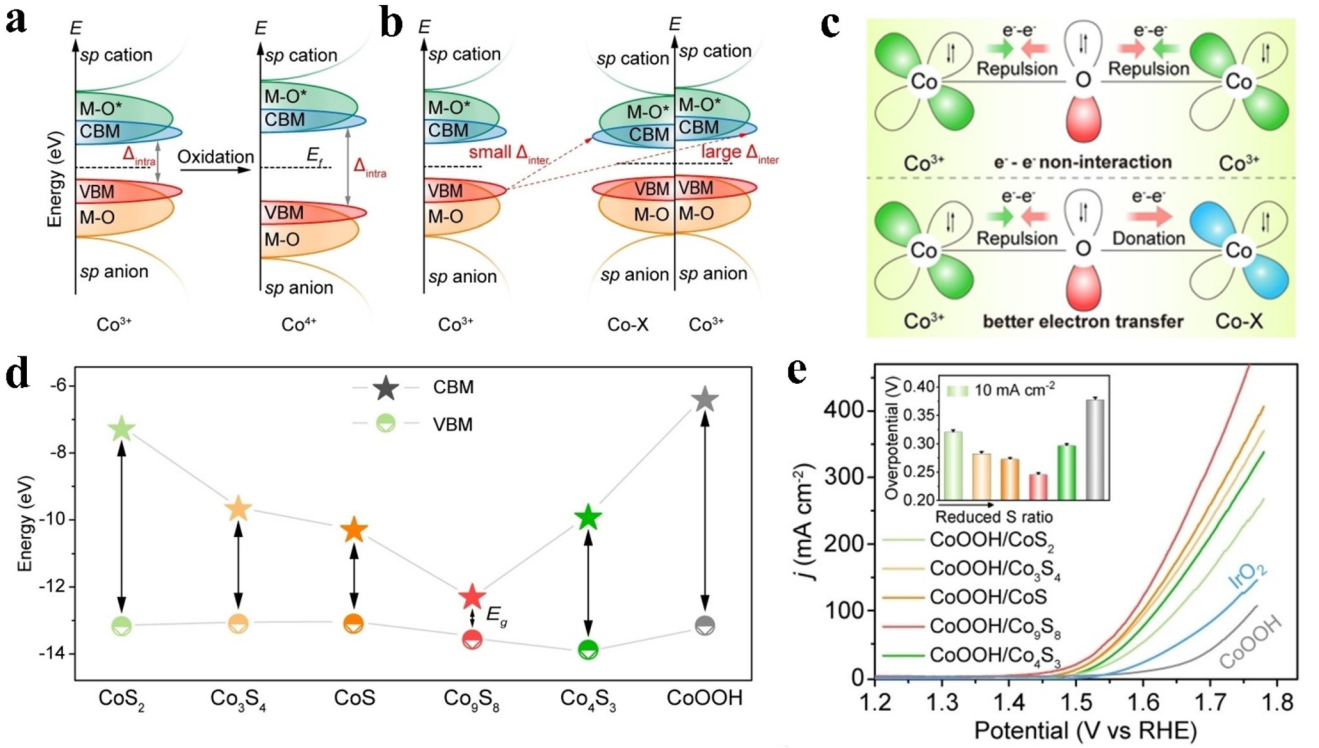

Fig. 6 (a) Schematic molecular orbital energy diagram for CoOOH and CoO_2, and the corresponding intramolecular energy gap (Δ_{intra}). (b) Intermolecular energy gap (Δ_{inter}) between the CBM and VBM in adjacent molecular orbitals of CoOOH, and between Co–X and CoOOH. (c) Representation of the electronic coupling on adjacent Co–O–Co in CoOOH and CoOOH/Co–X. (d) Energy value of CBM and VBM based on the Kohn–Sham (KS) orbital energy-level diagram for CoS_2, Co_3S_4, CoS, Co_9S_8, Co_4S_3 and CoOOH. (e) LSV curves of $CoOOH/CoS_\alpha$ samples, CoOOH and IrO_2 in 1 M KOH in an oxygen-saturated atmosphere (inset: corresponding overpotential at 10 mA cm^{-2}). Reproduced with permission from ref. 55: Copyright 2022, Wiley-VCH.

5. Summary and outlook

The development of OERs is inseparable from the introduction of *in situ*/*operando* testing techniques, which leads the research closer to the truth of OER mechanism. *In situ*/*operando* characterization technology has played a key role in the study of OER catalysts from the initial mechanism speculation to the present mechanism revelation, particularly in the confirmation of active sites. Different from the previous report that the metal is the active site in OERs, more accurately, the metastable high-valence metal sites, which are obtained by metal-site transformations induced by applied potentials, are the real, highly efficient catalytic active sites. With the support of *in situ* characterization technology, recently the high-valence transformation process of metal sites has been widely reported, and has received enough attention, which is considered to be an important optimization factor to be taken into account in the catalyst design. Meanwhile, these results are conducive to a deeper understanding of the catalyst active site, so as to provide new ideas for the design of new catalysts. Although significant progress has been made in exploring high-state active site transformation (construction), there are still opportunities and challenges for further development (Fig. 7).

(1) Lack of high-resolution *in situ* characterization technology. At present, *in situ* technology is the best way to directly reveal the change trend of the active site on the catalyst with the increase in the applied overpotential during the reaction process. However, the current data collection time for the *in situ* technology is not satisfactory, whereas the surface transformation of the catalyst during the electrochemical process often occurs in microseconds or even less. Therefore, the current technology cannot meet the needs of capturing the microscopic transformation process on the catalyst surface. It hinders the deeper exploration of the OER mechanism.

(2) *In situ* characterization technology are not conducive to widespread use, so it is important to find direct descriptors to evaluate the construction of high-valence sites. An effective descriptor relationship is introduced to establish the relationship between the electronic structure of catalysts and the construction of high-valence sites. It can not only be used for indirect proof of the construction of high-valence active sites without *in situ* characterization, but also provide effective ideas on the descriptors for the design of catalysts.

(3) To achieve efficient conversion of the active site, more reactive factors need to be considered. For example, the relationship between electrochemical active sites (based on Cdl assessment) and the final high-valence conversion site needs to be identified. The potential difference between the high-valence conversion potential and the onset potential affects the accuracy of the kinetic assessment based on the Tafel slope. More details will be revealed, which also means closer to the truth of the OER, while it provides more models and ideas for the further design of efficient catalysts.

By solving the above-mentioned problems, an efficient catalyst design idea based on the construction of high-valence active site will be obtained, which can be used for the rational design of OER electrocatalysts. Continuous advances in *in situ* characterization technology will certainly help to further reveal the dynamic changes of catalysts during the OER process, thereby advancing our understanding of real electrocatalytic processes and further paving the way for green energy applications based on electrocatalytic technologies.

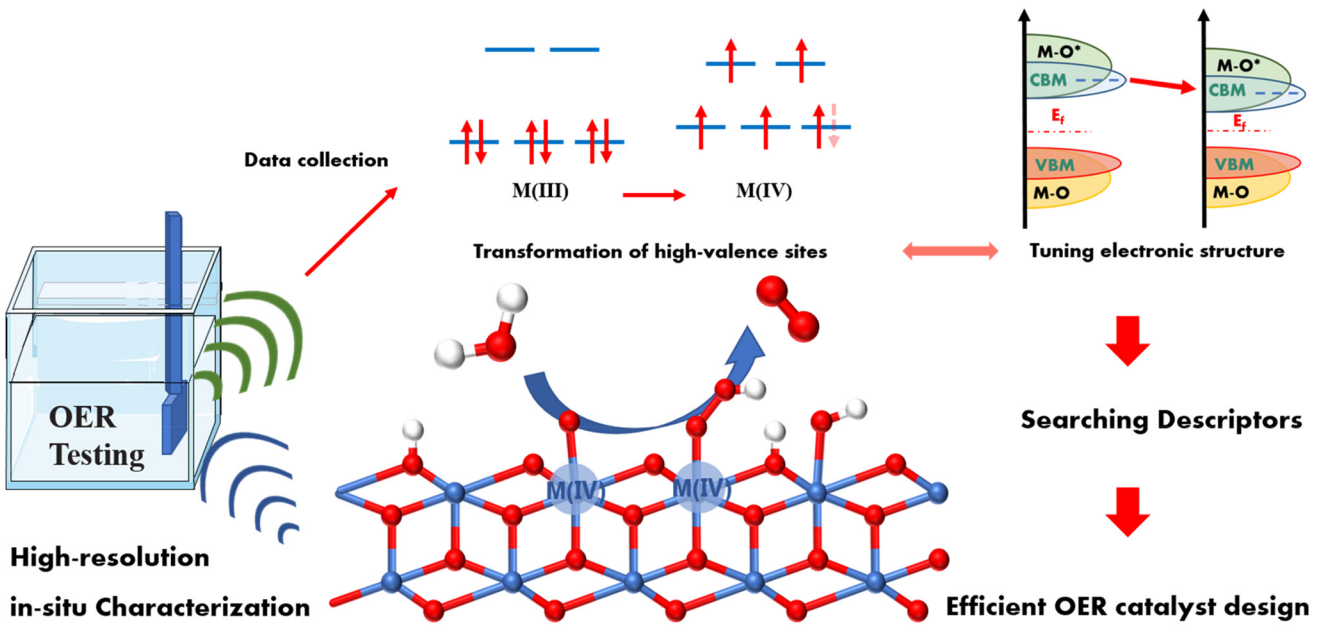

Fig. 7 Overview of the high-efficiency OER catalyst design based on the transformation mechanism of high-valence metal sites.

Author contributions

C. Qiao, C. B. Cao and J. T. Zhang designed and outlined the draft of the review paper. C. Qiao and Y. Y. Hao contributed to the scientific writing of the manuscript. All authors contributed to the final polishing of the manuscript.

Conflicts of interest

There are no conflicts to declare.

Acknowledgements

This study was financially supported by the National Natural Science Foundation of China (52272186, 51872030, 51702016, 51902023 and 21801015). We thank Analysis & Testing Center, Beijing Institute of Technology, for assistance.

References

1 L. Sharma, N. K. Katiyar, A. Parui, R. Das, R. Kumar, C. S. Tiwary, A. K. Singh, A. Halder and K. Biswas, *Nano Res.*, 2022, **15**, 4799–4806.
2 H. Yang, F. Li, S. Zhan, Y. Liu, W. Li, Q. Meng, A. Kravchenko, T. Liu, Y. Yang, Y. Fang, L. Wang, J. Guan, I. Furó, M. S. G. Ahlquist and L. Sun, *Nat. Catal.*, 2022, **5**, 414–429.
3 Z.-J. Zhao, S. Liu, S. Zha, D. Cheng, F. Studt, G. Henkelman and J. Gong, *Nat. Rev. Mater.*, 2019, **4**, 792–804.
4 J. Zhang, B. Cui, S. Jiang, H. Liu and M. Dou, *Nanoscale*, 2022, **14**, 9849–9859.
5 T. Yang, F. Qin, S. Zhang, H. Rong, W. Chen and J. Zhang, *Chem. Commun.*, 2021, **57**, 2164–2167.
6 H. Shang, Z. Jiang, D. Zhou, J. Pei, Y. Wang, J. Dong, X. Zheng, J. Zhang and W. Chen, *Chem. Sci.*, 2020, **11**, 5994–5999.
7 C. Qiao, S. Rafai, T. Cao, Z. Wang, H. Wang, Y. Zhu, X. Ma, P. Xu and C. Cao, *ChemCatChem*, 2020, **12**, 2823–2832.
8 Q. Wu, S. Wang, J. Guo, X. Feng, H. Li, S. Lv, Y. Zhou and Z. Chen, *Nano Res.*, 2022, **15**, 1901–1908.
9 D. Guo, X. Li, Y. Jiao, H. Yan, A. Wu, G. Yang, Y. Wang, C. Tian and H. Fu, *Nano Res.*, 2022, **15**, 238–247.
10 Q. Ye, J. Liu, L. Lin, M. Sun, Y. Wang and Y. Cheng, *Nanoscale*, 2022, **14**, 6648–6655.
11 H. Shang, W. Chen, Z. Jiang, D. Zhou and J. Zhang, *Chem. Commun.*, 2020, **56**, 3127–3130.
12 L. Meng, E. Zhang, H. Peng, Y. Wang, D. Wang, H. Rong and J. Zhang, *ChemCatChem*, 2022, **14**, e202101801.
13 R. Souleymen, Z. Wang, C. Qiao, M. Naveed and C. Cao, *J. Mater. Chem. A*, 2018, **6**, 7592–7607.
14 T. Wu, X. Ren, Y. Sun, S. Sun, G. Xian, G. G. Scherer, A. C. Fisher, D. Mandler, J. W. Ager, A. Grimaud, J. Wang, C. Shen, H. Yang, J. Gracia, H.-J. Gao and Z. J. Xu, *Nat. Commun.*, 2021, **12**, 3634.
15 Z. Qin, Z. Wang and J. Zhao, *Nanoscale*, 2022, **14**, 6902–6911.
16 X. Wan, Y. Song, H. Zhou and M. Shao, *Energy Mater. Adv.*, 2022, **2022**, 9842610.
17 H. Shang, T. Wang, J. Pei, Z. Jiang, D. Zhou, Y. Wang, H. Li, J. Dong, Z. Zhuang, W. Chen, D. Wang, J. Zhang and Y. Li, *Angew. Chem., Int. Ed.*, 2020, **59**, 22465–22469.
18 L.-H. Liu, N. Li, M. Han, J.-R. Han and H.-Y. Liang, *Rare Met.*, 2022, **41**, 125–131.
19 Z. Huang, Z. Yang, Q. Jia, N. Wang, Y. Zhu and Y. Xia, *Nanoscale*, 2022, **14**, 4726–4739.
20 H. Gu, X. Li, J. Zhang and W. Chen, *Small*, 2022, **18**, 2105883.
21 H. Gu, W. Chen and X. Li, *J. Mater. Chem. A*, 2022, **10**, 22331–22353.
22 K. Yin, Y. Chao, L. Zeng, M. Li, F. Liu, S. Guo and H. Li, *Energy Mater. Adv.*, 2022, **2022**, 9871842.
23 W. Tang, J. Jian, G. Chen, W. Bian, J. Yu, H. Wang, M. Zhou, D. Ding and H. Luo, *Energy Mater. Adv.*, 2021, **2021**, 8140964.
24 H. Shang, X. Zhou, J. Dong, A. Li, X. Zhao, Q. Liu, Y. Lin, J. Pei, Z. Li, Z. Jiang, D. Zhou, L. Zheng, Y. Wang, J. Zhou, Z. Yang, R. Cao, R. Sarangi, T. Sun, X. Yang, X. Zheng, W. Yan, Z. Zhuang, J. Li, W. Chen, D. Wang, J. Zhang and Y. Li, *Nat. Commun.*, 2020, **11**, 3049.
25 H. Li, L. Chen, P. Jin, Y. Li, J. Pang, J. Hou, S. Peng, G. Wang and Y. Shi, *Nano Res.*, 2022, **15**, 950–958.
26 Z. Zhao, Q. Shao, J. Xue, B. Huang, Z. Niu, H. Gu, X. Huang and J. Lang, *Nano Res.*, 2022, **15**, 310–316.
27 M. Wang, L. Zhang, J. Pan, M. Huang and H. Zhu, *Nano Res.*, 2021, **14**, 4740–4747.
28 Y. Qin, Z. Wang, W. Yu, Y. Sun, D. Wang, J. Lai, S. Guo and L. Wang, *Nano Lett.*, 2021, **21**, 5774–5781.
29 P. Song, P. Zhu, X. Su, M. Hou, D. Zhao and J. Zhang, *Chem. – Asian J.*, 2022, **17**, e202200716.
30 D. Zhao, K. Yu, P. Song, W. Feng, B. Hu, W.-C. Cheong, Z. Zhuang, S. Liu, K. Sun, J. Zhang and C. Chen, *Energy Environ. Sci.*, 2022, **15**, 3795–3804.
31 X. Ma, X.-Y. Zhang, M. Yang, J.-Y. Xie, R.-Q. Lv, Y.-M. Chai and B. Dong, *Rare Met.*, 2021, **40**, 1048–1055.
32 A. G. Rajan, J. M. P. Martirez and E. A. Carter, *J. Am. Chem. Soc.*, 2020, **142**, 3600–3612.
33 Y. Zhang, Z. Gu, J. Bi and Y. Jiao, *Nanoscale*, 2022, **14**, 10873–10879.
34 Q. Xu, H. Jiang, X. Duan, Z. Jiang, Y. Hu, S. W. Boettcher, W. Zhang, S. Guo and C. Li, *Nano Lett.*, 2021, **21**, 492–499.
35 Q. Wu, K. Jiang, J. Han, D. Chen, M. Luo, J. Lan, M. Peng and Y. Tan, *Sci. China Mater.*, 2022, **65**, 1262.
36 K. Zhang, Z. Zhang, H. Shen, Y. Tang, Z. Liang and R. Zou, *Sci. China Mater.*, 2022, **65**, 1522.
37 Y. Zhang, X. Teng, Z. Ma, R. Wang, W.-M. Lau and A. Shan, *Prog. Nat. Sci-Mater.*, 2022, **32**, 554–560.
38 X. Xie, L. Du, L. Yan, S. Park, Y. Qiu, J. Sokolowski, W. Wang and Y. Shao, *Adv. Funct. Mater.*, 2022, **32**, 2110036.

39 N. Jiang, Z. Zhu, W. Xue, B. Y. Xia and B. You, *Adv. Mater.*, 2022, **34**, 2105852.
40 M. Yu, E. Budiyanto and H. Tüysüz, *Angew. Chem., Int. Ed.*, 2022, **61**, e202103824.
41 H. A. Hansen, V. Viswanathan and J. K. Nørskov, *J. Phys. Chem. C*, 2014, **118**, 6706–6718.
42 Z. W. Seh, J. Kibsgaard, C. F. Dickens, I. Chorkendorff, J. K. Nørskov and T. F. Jaramillo, *Science*, 2017, **355**, eaad4998.
43 T. Bligaard, J. K. Nørskov, S. Dahl, J. Matthiesen, C. H. Christensen and J. Sehested, *J. Catal.*, 2004, **224**, 206–217.
44 K. S. Exner and H. Over, *Acc. Chem. Res.*, 2017, **50**, 1240–1247.
45 F.-Y. Chen, Z.-Y. Wu, Z. Adler and H. Wang, *Joule*, 2021, **5**, 1704–1731.
46 C. Qiao, Y. Zhang, Y. Zhu, C. Cao, X. Bao and J. Xu, *J. Mater. Chem. A*, 2015, **3**, 6878–6883.
47 M. Yan, K. Mao, P. Cui, C. Chen, J. Zhao, X. Wang, L. Yang, H. Yang, Q. Wu and Z. Hu, *Nano Res.*, 2020, **13**, 328–334.
48 T. Zhang, S. Zhao, C. Zhu, J. Shi, C. Su, J. Yang, M. Wang, J. Li, J. Li, P. Liu and C. Wang, *Nano Res.*, 2022, DOI: **10.1007/s12274-022-4879-2**.
49 J. Zhou, L. Zhang, Y.-C. Huang, C.-L. Dong, H.-J. Lin, C.-T. Chen, L. H. Tjeng and Z. Hu, *Nat. Commun.*, 2020, **11**, 1984.
50 K. Dang, S. Zhang, X. Wang, W. Sun, L. Wang, Y. Tian and S. Zhan, *Nano Res.*, 2021, **14**, 4848–4856.
51 J. Bak, H. B. Bae and S.-Y. Chung, *Nat. Commun.*, 2019, **10**, 2713.
52 M. Yan, Z. Zhao, P. Cui, K. Mao, C. Chen, X. Wang, Q. Wu, H. Yang, L. Yang and Z. Hu, *Nano Res.*, 2021, **14**, 4220–4226.
53 W. H. Lee, M. H. Han, Y.-J. Ko, B. K. Min, K. H. Chae and H.-S. Oh, *Nat. Commun.*, 2022, **13**, 605.
54 H. Chang, Z. Liang, L. Wang and C. Wang, *Nanoscale*, 2022, **14**, 5639–5656.
55 N. Yao, G. Wang, H. Jia, J. Yin, H. Cong, S. Chen and W. Luo, *Angew. Chem., Int. Ed.*, 2022, **61**, e202117178.
56 F. T. Haase, A. Rabe, F.-P. Schmidt, A. Herzog, H. S. Jeon, W. Frandsen, P. V. Narangoda, I. Spanos, K. F. Ortega, J. Timoshenko, T. Lunkenbein, M. Behrens, A. Bergmann, R. Schlögl and B. R. Cuenya, *J. Am. Chem. Soc.*, 2022, **144**, 12007–12019.
57 J. M. P. Martirez and E. A. Carter, *J. Am. Chem. Soc.*, 2019, **141**, 693–705.
58 K. Zhu, X. Zhu and W. Yang, *Angew. Chem., Int. Ed.*, 2019, **58**, 1252–1265.
59 Y. Deng and B. S. Yeo, *ACS Catal.*, 2017, **7**, 7873–7889.
60 L. Gao, X. Cui, C. D. Sewell, J. Li and Z. Lin, *Chem. Soc. Rev.*, 2021, **50**, 8428–8469.
61 J. Wang, Y. Gao, H. Kong, J. Kim, S. Choi, F. Ciucci, Y. Hao, S. Yang, Z. Shao and J. Lim, *Chem. Soc. Rev.*, 2020, **49**, 9154–9196.
62 H.-Y. Wang, S.-F. Hung, H.-Y. Chen, T.-S. Chan, H. M. Chen and B. Liu, *J. Am. Chem. Soc.*, 2016, **138**, 36–39.
63 J. Zhou, Y. Wang, X. Su, S. Gu, R. Liu, Y. Huang, S. Yan, J. Li and S. Zhang, *Energy Environ. Sci.*, 2019, **12**, 739–746.
64 A. Moysiadou, S. Lee, C.-S. Hsu, H. M. Chen and X. Hu, *J. Am. Chem. Soc.*, 2020, **142**, 11901–11914.
65 E. Fabbri, M. Nachtegaal, T. Binninger, X. Cheng, B.-J. Kim, J. Durst, F. Bozza, T. Graule, R. Schäublin, L. Wiles, M. Pertoso, N. Danilovic, K. E. Ayers and T. J. Schmidt, *Nat. Mater.*, 2017, **16**, 925–931.
66 W. Wan, Y. Zhao, S. Wei, C. A. Triana, J. Li, A. Arcifa, C. S. Allen, R. Cao and G. R. Patzke, *Nat. Commun.*, 2021, **12**, 5589.
67 M. Görlin, J. H. Stenlid, S. Koroidov, H.-Y. Wang, M. Börner, M. Shipilin, A. Kalinko, V. Murzin, O. V. Safonova, M. Nachtegaal, A. Uheida, J. Dutta, M. Bauer, A. Nilsson and O. Diaz-Morales, *Nat. Commun.*, 2020, **11**, 6181.
68 D. Friebel, M. W. Louie, M. Bajdich, K. E. Sanwald, Y. Cai, A. M. Wise, M.-J. Cheng, D. Sokaras, T.-C. Weng, R. Alonso-Mori, R. C. Davis, J. R. Bargar, J. K. Nørskov, A. Nilsson and A. T. Bell, *J. Am. Chem. Soc.*, 2015, **137**, 1305–1313.
69 J. Y. C. Chen, L. Dang, H. Liang, W. Bi, J. B. Gerken, S. Jin, E. E. Alp and S. S. Stahl, *J. Am. Chem. Soc.*, 2015, **137**, 15090–15093.
70 D. Wang, J. Zhou, Y. Hu, J. Yang, N. Han, Y. Li and T. K. Sham, *J. Phys. Chem. C*, 2015, **119**, 19573–19583.
71 M. Görlin, P. Chernev, J. F. de Araújo, T. Reier, S. Dresp, B. Paul, R. Krähnert, H. Dau and P. Strasser, *J. Am. Chem. Soc.*, 2016, **138**, 5603–5614.
72 H. Xiao, H. Shin and W. A. Goddard, *Proc. Natl. Acad. Sci. U. S. A.*, 2018, **115**, 5872–5877.
73 H. Shin, H. Xiao and W. A. Goddard, *J. Am. Chem. Soc.*, 2018, **140**, 6745–6748.
74 A. J. Tkalych, K. Yu and E. A. Carter, *J. Phys. Chem. C*, 2015, **119**, 24315–24322.
75 X. Zheng, B. Zhang, P. De Luna, Y. Liang, R. Comin, O. Voznyy, L. Han, F. P. G. de Arquer, M. Liu, C. T. Dinh, T. Regier, J. J. Dynes, S. He, H. L. Xin, H. Peng, D. Prendergast, X. Du and E. H. Sargent, *Nat. Chem.*, 2018, **10**, 149–154.
76 N. Zhang, X. Feng, D. Rao, X. Deng, L. Cai, B. Qiu, R. Long, Y. Xiong, Y. Lu and Y. Chai, *Nat. Commun.*, 2020, **11**, 4066.
77 Z.-W. Gao, J.-Y. Liu, X.-M. Chen, X.-L. Zheng, J. Mao, H. Liu, T. Ma, L. Li, W.-C. Wang and X.-W. Du, *Adv. Mater.*, 2019, **31**, 1804769.
78 B. Zhang, L. Wang, Z. Cao, S. M. Kozlov, F. P. G. de Arquer, C. T. Dinh, J. Li, Z. Wang, X. Zheng, L. Zhang, Y. Wen, O. Voznyy, R. Comin, P. De Luna, T. Regier, W. Bi, E. E. Alp, C.-W. Pao, L. Zheng, Y. Hu, Y. Ji, Y. Li, Y. Zhang, L. Cavallo, H. Peng and E. H. Sargent, *Nat. Catal.*, 2020, **3**, 985–992.
79 C. Qiao, Z. Usman, T. Cao, S. Rafai, Z. Wang, Y. Zhu, C. Cao and J. Zhang, *Chem. Eng. J.*, 2021, **426**, 130873.

80 S. Zhao, C. Tan, C. T. He, P. An, F. Xie, S. Jiang, Y. Zhu, K.-H. Wu, B. Zhang, H. Li, J. Zhang, Y. Chen, S. Liu, J. Dong and Z. Tang, *Nat. Energy*, 2020, **5**, 881–890.
81 T. Wu, S. Sun, J. Song, S. Xi, Y. Du, B. Chen, W. A. Sasangka, H. Liao, C. L. Gan, G. G. Scherer, L. Zeng, H. Wang, H. Li, A. Grimaud and Z. J. Xu, *Nat. Catal.*, 2019, **2**, 763–772.
82 C. Huang, Q. Zhou, D. Duan, L. Yu, W. Zhang, Z. Wang, J. Liu, B. Peng, P. An, J. Zhang, L. Li, J. Yu and Y. Yu, *Energy Environ. Sci.*, 2022, **15**, 4647–4658.
83 Y. Zhao, W. Wan, N. Dongfang, C. A. Triana, L. Douls, C. Huang, R. Erni, M. Iannuzzi and G. R. Patzke, *ACS Nano*, 2022, **16**, 15318–15327.